

# Local Wavelet Pattern: A New Feature Descriptor for Image Retrieval in Medical CT Databases

Shiv Ram Dubey, *Student Member, IEEE*, Satish Kumar Singh, *Senior Member, IEEE*,  
and Rajat Kumar Singh, *Senior Member, IEEE*

**Abstract**— A new image feature description based on the local wavelet pattern (LWP) is proposed in this paper to characterize the medical CT images for content-based CT image retrieval. In the proposed work, the LWP is derived for each pixel of the CT image by utilizing the relationship of centre pixel with the local neighboring information. In contrast to the Local Binary Pattern which only considers the relationship between a centre pixel and its neighboring pixels, presented approach first utilizes the relationship among the neighboring pixels using local wavelet decomposition and finally considers its relationship with the centre pixel. A centre pixel transformation scheme is introduced to match the range of centre value with the range of local wavelet decomposed values. Moreover, the introduced local wavelet decomposition scheme is centrally symmetric and suitable for CT images. The novelty of this manuscript lies in following two ways, (1) encoding local neighboring information with local wavelet decomposition and (2) computing LWP using local wavelet decomposed values and transformed centre pixel values. We tested the performance of our method over three CT image databases in terms of the precision and recall. We also compared proposed LWP descriptor with other state-of-the-art local image descriptors and the experimental results suggest that the proposed method outperforms other methods for CT image retrieval.

**Index Terms**—Medical diagnosis, CT images, Image retrieval, Local image descriptors, Local wavelet pattern, LBP, LTP.

## I. INTRODUCTION

### A. Motivation

IN the field of medical analysis, images play a crucial role for management, diagnosis and teaching purposes. Now various types of images are being generated by the medical imaging devices such as computer tomography (CT), magnetic resonance imaging (MRI), visible, nuclear imaging, etc. to capture the patient pathology [1]. These images may be treated

as a source for the diagnosis aid. However due to the rapid increase in the number of medical images day by day, the patient diagnosis in medical institutions and hospitals is becoming more challenging and required more accurate and efficient image searching, indexing and retrieving methods. Content-based image indexing and retrieval is turning up continuously to combat this problem on the basis of the image digital content [2] such as color, texture, shape, structure, etc. The extensive and comprehensive literature survey on content based image retrieval (CBIR) is presented in [3]-[4]. Medical image retrieval systems are being used mostly by the physicians to point out the disorder present in the patient image by retrieving the most similar images from the related reference images with its associated information. The existing medical image retrieval systems are presented by various researchers through the published literature [5]-[11]. Muller et al. have reviewed the medical CBIR approaches on the basis of the clinical benefits [12].

The feature vectors are extracted from each image in order to facilitate the image retrieval and the feature vector of query image is compared with the feature vectors of the database images. The performance and efficiency of any CBIR system is heavily dependent upon the feature vectors [28]. The feature vectors being used in recent retrieval and classification systems utilize the visual information of the image such as shape [13]-[14], texture [15]-[16], [43], edges [17]-[18], color histograms [19]-[20], etc. Texture based image descriptors have been widely used in the field of pattern recognition to capture the fine details of the image. In this paper, we presented a local wavelet texture feature for medical CT image retrieval.

### B. Related Work

Ojala et al. [21] introduced the local binary pattern (LBP) for texture classification. LBP operator became more popular due to its reduced computational complexity and enhanced performance in several applications such as face recognition [22], analysis of facial paralysis [23], analysis of pulmonary emphysema [24], etc. Several other LBP variants [25]-[27], [45]-[49] also proposed for texture representation in view of high success of LBP. Centre symmetric local binary pattern is investigated to reduce the dimension of the LBP for local region matching [26]. Local ternary pattern (LTP) is introduced as the generalization of LBP for face recognition under varying lighting situations [27]. These methods are generally illumination invariant. Peng et al. extracted the

Copyright (c) 2015 IEEE. Personal use of this material is permitted. Permission from IEEE must be obtained for all other users, including reprinting/ republishing this material for advertising or promotional purposes, creating new collective works for resale or redistribution to servers or lists, or reuse of any copyrighted components of this work in other works.

The authors are with the Indian Institute of Information Technology Allahabad, India (e-mail: shivram1987@gmail.com, sk.singh@iitaa.ac.in, rajatsingh@iitaa.ac.in).

The final paper is available from: <http://dx.doi.org/10.1109/TIP.2015.2493446>

texture cues in chest CT images on the basis of the uniformity of structure and brightness in the image [29]. They depicted the structure and brightness in the image using extended rotation invariant local binary pattern and difference in gradient orientations. Two descriptors namely local diagonal extrema pattern [44] and local bit-plane decoded pattern [50] are investigated very recently for biomedical images. Region of interest retrieval is proposed by Unay et al. [30] in brain MR images on the basis of the local structure exist in the image. SVM-based feature selection is applied over the textural features for tumor recognition [31] in wireless capsule endoscopy images. Felipe et al. have used the co-occurrence based gradient texture feature for tissue identification by CBIR system [32]. To reduce the memory required for image storage, physiological kinetic feature is presented by Cai et al. [33] for positron-emission-tomography (PET) image retrieval. Some methods designed for medical image retrieval using distance metric/similarity learning are depicted in [34]-[36]. Wavelet based features are also presented by some researchers in medical CBIR systems [37]-[38]. These methods mainly used the wavelet transformation over the images globally [39] (i.e. 2-D wavelet transformation of image) whereas we applied the wavelet decomposition technique locally using 1-D Haar wavelet transformation which is more advantageous to encode the local texture information.

### C. Major Contribution

The local feature descriptions presented through the published literature have utilized the relationship of a referenced pixel with its neighboring pixel [15], [21], [27]. Some approaches also tried to utilize the relationship among the neighboring pixels with success in some extent but at the expense of high dimensionality which are generally more time consuming for image retrieval [17]. This is the motivation for us to propose a new local wavelet pattern (LWP) based feature vector of low dimension. LWP uses both relationship i.e. among local neighbors and also between the centre pixel and its local neighbors to construct the descriptor. It encodes the relationship among the local neighbors using local wavelet decomposition method and finally produces a binary pattern by comparing these decomposed values with the transformed centre pixel value. The outperformance and efficiency of the LWP has been made confirmed through medical image retrieval experiments over three CT databases.

The remaining of the manuscript is integrated in following manner. Section II presents the proposed framework of CT image retrieval and also proposed the construction of LWP feature vector. Section III describes the evaluation criteria. In Section IV, experiments are performed while result analysis and discussions are presented in section V and finally concluding remarks are highlighted in Section VI.

## II. MEDICAL CT IMAGE RETRIEVAL FRAMEWORK

In this section, we present the framework for medical CT image retrieval using local wavelet pattern (LWP). Fig. 1 shows the proposed framework using block diagrams.

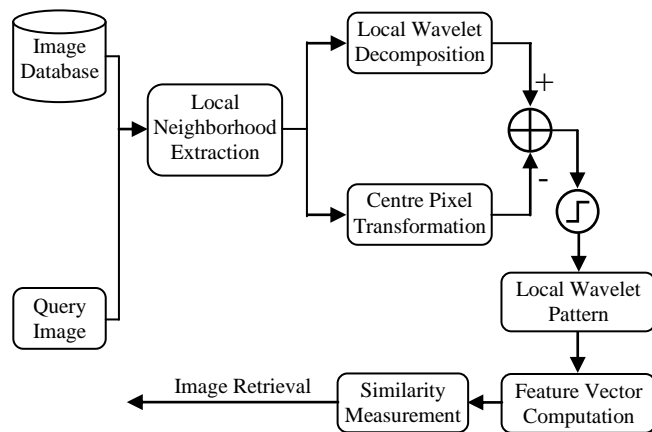


Fig. 1. Proposed system framework for medical CT image retrieval.

Local neighborhood extraction, local wavelet decomposition, centre pixel transformation, local wavelet pattern generation, feature vector generation, similarity measurement, and image retrieval are the main processing units of the proposed CT image retrieval. In this section, first the extraction process of local neighborhood of any given centre pixel  $P^{i,j}$  at co-ordinate  $(i, j)$  of any grayscale CT image  $M$  of dimension  $m_1 \times m_2$  is described, then we will present the concept of local wavelet decomposition of extracted local neighborhood and centre pixel transformation, then the construction of local wavelet pattern is introduced and after construction of local wavelet pattern for each of the pixel of the image, the feature vector for that image is generated. Now the query image will be matched with the database images by comparing its feature vector with the feature vectors of the database images and most similar images will be retrieved.

### A. Local Neighborhood Extraction

To facilitate the computation of local wavelet pattern (LWP), first we required to extract the local neighborhood of any given pixel. We extract the local neighbors in a manner such that all the extracted neighbors will be equally spaced at a particular radius from the centre pixel similar to [16], [22], [25]. Let  $M$  is a grayscale CT image of dimension  $m_1 \times m_2$ . The  $P^{i,j}$  is a particular pixel of image  $M$  at coordinate  $(i, j)$  in Cartesian coordinate system having origin at left and upper corner of the image as shown in Fig. 2 and the intensity value at pixel  $P^{i,j}$  is  $I^{i,j}$ .

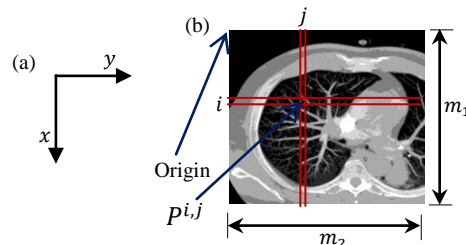


Fig. 2. (a) The axis of the image in Cartesian coordinate system, and (b) the origin of the axis is at the upper and left corner of the image and  $P^{i,j}$  is the pixel of image at coordinate  $(i, j)$ .

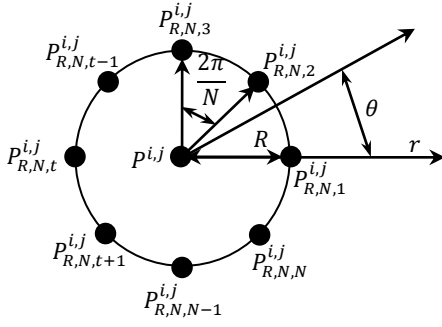


Fig. 3. The local neighbors (i.e.  $P_{R,N,t}^{i,j}$  for  $\forall t \in [1, N]$ ) of a centre pixel ( $P^{i,j}$ ) in polar coordinate system.

We represented  $P_{R,N}^{i,j}$  to denote the set of  $N$  local neighbors of  $P^{i,j}$  equally distributed at a circle of radius  $R$  having centre at  $P^{i,j}$ . As depicted in Fig. 3, the  $t^{th}$  neighbor of  $P^{i,j}$  (i.e.  $t^{th}$  element of  $P_{R,N}^{i,j}$ ) is denoted as  $P_{R,N,t}^{i,j}$  having intensity value  $I_{R,N,t}^{i,j}$  where  $t$  is positive integer and  $t \in [1, N]$ . It should be noted that we can consider only those pixels as a central pixel whose all  $N$  local neighbors' co-ordinate are within the dimension of the image  $M$ . The coordinate of  $P_{R,N,t}^{i,j}$  with respect to the origin of the image in Cartesian coordinate  $(x, y)$  system is given as,

$$x(P_{R,N,t}^{i,j}) = i - r(P_{R,N,t}^{i,j}) \times \sin(\theta(P_{R,N,t}^{i,j})) \quad (1)$$

$$y(P_{R,N,t}^{i,j}) = j + r(P_{R,N,t}^{i,j}) \times \cos(\theta(P_{R,N,t}^{i,j})) \quad (2)$$

where  $i \in [R + 1, m_1 - R]$ ,  $j \in [R + 1, m_2 - R]$ ,  $r(P_{R,N,t}^{i,j})$  and  $\theta(P_{R,N,t}^{i,j})$  are the coordinates of  $P_{R,N,t}^{i,j}$  in the polar coordinate system w.r.t. the  $P^{i,j}$  and computed as,

$$r(P_{R,N,t}^{i,j}) = R \quad (3)$$

$$\theta(P_{R,N,t}^{i,j}) = (t - 1) \times \frac{2\pi}{N} \quad (4)$$

### B. Local Wavelet Decomposition

The  $N$  neighbors at radius  $R$  of any pixel  $P^{i,j}$  are  $P_{R,N,t}^{i,j}$  having intensity value  $I_{R,N,t}^{i,j}$  where  $t \in [1, N]$ . Now, we use these intensity values to encode the relationship existing among the neighbors of the centre pixel using the concept of local wavelet decomposition. We applied 1-D Haar wavelet decomposition to transform the  $I_{R,N,t}^{i,j}$  into  $W_{R,N,t}^{i,j,l}$  for  $\forall t \in [1, N]$ , where  $l$  is a positive integer number (i.e.  $l \in \mathbb{N}^+$ ) used to represent the level of transformation. Note that the value of  $N$  should be chosen in such a way that it satisfies the following criteria,

$$\text{mod}(N, 2^l) = 0 \quad (5)$$

where  $\text{mod}(a_1, a_2)$  is a function to find the remainder when  $a_1$  is divided by  $a_2$ , and the maximum possible value of  $l$  (i.e.  $l_{max}$ ) depends upon the total number of neighbors ( $N$ ) under consideration and satisfies the following criteria,

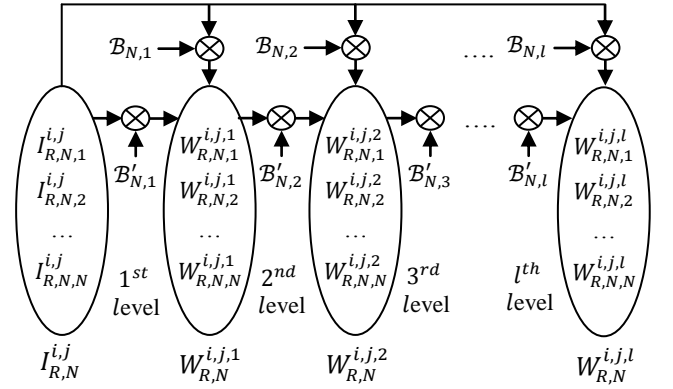


Fig. 4. The transformation of an  $N$ -dimensional vector  $I_{R,N}^{i,j}$  to another  $N$ -dimensional vector  $W_{R,N}^{i,j,l}$  at  $l^{th}$  level.

$$2^{l_{max}-1} \leq N \leq 2^{l_{max}} \quad (6)$$

Let  $I_{R,N}^{i,j} = \{(I_{R,N,1}^{i,j}, I_{R,N,2}^{i,j}, \dots, I_{R,N,N}^{i,j}) : I_{R,N,t}^{i,j} \in \mathbb{R}\}$  and  $W_{R,N}^{i,j,l} = \{(W_{R,N,1}^{i,j,l}, W_{R,N,2}^{i,j,l}, \dots, W_{R,N,N}^{i,j,l}) : W_{R,N,t}^{i,j,l} \in \mathbb{R}\}$  be the two sets of  $N$ -dimensional vectors, where  $I_{R,N,t}^{i,j}$  is the intensity value of the  $t^{th}$  neighbor and  $W_{R,N,t}^{i,j,l}$  is the  $t^{th}$  wavelet decomposed value at  $l^{th}$  level. We defined a function  $f_1 : (I_{R,N}^{i,j}, l) \rightarrow W_{R,N}^{i,j,l}$  to transform an  $N$ -dimensional vector  $I_{R,N}^{i,j}$  at  $l^{th}$  level to another  $N$ -dimensional vector  $W_{R,N}^{i,j,l}$  based on the basis function of the 1-D Haar wavelet at that level as shown in Fig. 4. Mathematically, this transformation is defined as,

$$W_{R,N}^{i,j,l} = f_1(I_{R,N}^{i,j}, l) \quad (7)$$

where function  $f_1$  uses a recursive basis function  $\mathcal{B}_{N,l}$  with  $I_{R,N}^{i,j}$  to find  $W_{R,N}^{i,j,l}$  as follows,

$$f_1(I_{R,N}^{i,j}, l) = (\mathcal{B}_{N,l} \times (I_{R,N}^{i,j})^T)^T \quad (8)$$

From (7) and (8),  $W_{R,N}^{i,j,l}$  can be represented in the terms of  $\mathcal{B}_{N,l}$  and  $I_{R,N}^{i,j}$  as,

$$W_{R,N}^{i,j,l} = (\mathcal{B}_{N,l} \times (I_{R,N}^{i,j})^T)^T \quad (9)$$

where  $\mathcal{B}_{N,l}$  is the basis function at  $l^{th}$  level for  $N$  values and given as,

$$\mathcal{B}_{N,l} = \begin{cases} \mathcal{B}'_{N,l} \times \mathcal{B}_{N,l-1} & \text{If } 1 \leq l \leq l_{max} \\ U_N & \text{If } l = 0 \end{cases} \quad (10)$$

where  $U_N$  is the unit matrix of size  $N \times N$ ,  $\mathcal{B}_{N,l-1}$  is the basis function at  $(l-1)^{th}$  level and  $\mathcal{B}'_{N,l}$  is the 1-D Haar wavelet square basis matrix of size  $N \times N$  for  $l^{th}$  level transformation. Note that in (9) the basis matrix  $\mathcal{B}_{N,l}$  is computed recursively from the  $\mathcal{B}_{N,l-1}$  and directly applied with input values  $I_{R,N}^{i,j}$  to obtain the  $W_{R,N}^{i,j,l}$ . Further in this section, we show that  $W_{R,N}^{i,j,l}$  can also be obtained recursively from  $W_{R,N}^{i,j,l-1}$  without recursive computation of  $\mathcal{B}_{N,l}$  instead by using the basis matrix of  $l^{th}$  level (i.e.  $\mathcal{B}'_{N,l}$ ) only.

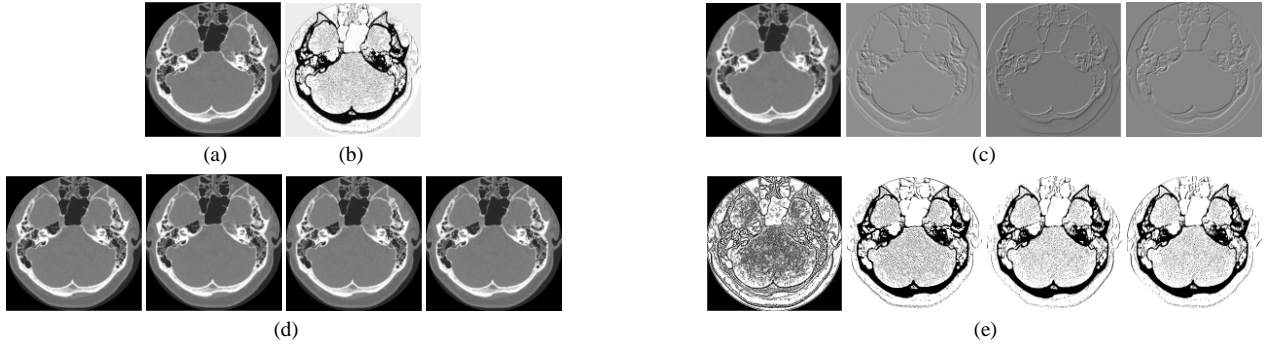


Fig. 5. An example image considered from the Nema-CT database to show the effect of each step. (a) Considered Image, (b) the final local wavelet pattern map of image, (c) local wavelet decomposed images for  $t = 1, 2, 3$ , and 4 respectively while  $l = 2$ ,  $R = 1$  and  $N = 4$ , (d) centre pixel transformed images for  $t = 1, 2, 3$ , and 4 respectively, and (e) local wavelet patterns for  $t = 1, 2, 3$ , and 4 respectively.

The values of the elements of matrix  $\mathcal{B}'_{N,l}$  depends upon the level of transformation (i.e.  $l$ ) and defined as follows,

$$\mathcal{B}'_{N,l}(u, v) = \begin{cases} \frac{1}{\sqrt{2}} & \text{If } (C_1 \text{ and } C_2) \text{ or } (C_3 \text{ and } C_4) \\ -\frac{1}{\sqrt{2}} & \text{If } C_3 \text{ and } C_5 \\ 1 & \text{If } C_6 \\ 0 & \text{Else} \end{cases} \quad (11)$$

where  $u$  and  $v$  are the row and column number of the matrix  $\mathcal{B}'_{N,l}$  (i.e.  $u \in [1, N]$  and  $v \in [1, N]$ ) and  $C_\gamma$  are the different conditions for  $\gamma = 1, 2, \dots, 6$  and defined on the basis of the  $u$ ,  $v$ ,  $l$  and  $N$  as follows,

$$C_\gamma = \begin{cases} 1 \leq u \leq \frac{N}{2^l}, & \gamma = 1 \\ (v = 2u - 1) \text{ or } (v = 2u), & \gamma = 2 \\ \frac{N}{2^l} + 1 \leq u \leq \frac{N}{2^{l-1}}, & \gamma = 3 \\ v = 2u - \frac{N}{2^{l-1}} - 1, & \gamma = 4 \\ v = 2u - \frac{N}{2^{l-1}}, & \gamma = 5 \\ \left(u \geq \frac{N}{2^{l-1}} + 1\right) \text{ and } (v = u), & \gamma = 6 \end{cases} \quad (12)$$

From (9) and (10), we can write  $W_{R,N}^{i,j,l}$  in the following form,

$$W_{R,N}^{i,j,l} = \begin{cases} (\mathcal{B}'_{N,l} \times \mathcal{B}_{N,l-1} \times (I_{R,N}^{i,j})^T)^T & \text{If } 1 \leq l \leq l_{max} \\ (U_N \times (I_{R,N}^{i,j})^T)^T & \text{If } l = 0 \end{cases} \quad (13)$$

After replacing  $\mathcal{B}_{N,l-1} \times (I_{R,N}^{i,j})^T$  with  $(W_{R,N}^{i,j,l-1})^T$  from (9) in (13) and simplifying (13), we find that  $W_{R,N}^{i,j,l}$  can be defined recursively in following manner,

$$W_{R,N}^{i,j,l} = \begin{cases} (\mathcal{B}'_{N,l} \times (W_{R,N}^{i,j,l-1})^T)^T & \text{If } 1 \leq l \leq l_{max} \\ I_{R,N}^{i,j} & \text{If } l = 0 \end{cases} \quad (14)$$

where  $W_{R,N}^{i,j,l-1}$  is an  $N$ -dimensional vector obtained after 1-D Haar wavelet decomposition of  $I_{R,N}^{i,j}$  at  $(l-1)^{th}$  level.

We also depicted 4 local decomposed images (i.e.  $W_{4,4,t}^2$ ) in Fig. 5(c) for an example image of Fig. 5(a). These 4 images correspond to the  $t = 1, 2, 3$ , and 4 when we considered  $l = 2$ ,  $R = 4$  and  $N = 4$ . It can be seen that these images are having varying degree of information associated after local wavelet decomposition which will be used with the centre pixel information to encode the feature vector.

### C. Centre Pixel Transformation

We encoded the relationship among the neighboring pixels  $P_{R,N}^{i,j}$  of the centre pixel  $P^{i,j}$  using local wavelet decomposition in the previous section. But, finally we have to encode the relationship exist between  $P^{i,j}$  and  $P_{R,N}^{i,j}$ . Most of the existing methods have used directly the intensity values of the neighboring pixels ( $I_{R,N}^{i,j}$ ), whereas we will use the local wavelet decomposed values at level  $l$  of the neighboring pixels (i.e.  $W_{R,N}^{i,j,l}$ ) for this purpose to compare with the  $I^{i,j}$ . It is obvious that, we can't compare  $W_{R,N}^{i,j,l}$  with  $I^{i,j}$  directly because the range of the values of  $W_{R,N}^{i,j,l}$  is now changed. To cope with this problem, we propose a centre pixel transformation scheme which transforms  $I^{i,j}$  into an array  $\tau_{N,t}^{i,j,l}$  of length  $N$  at level  $l$  such that the range of the  $\tau_{N,t}^{i,j,l}$  is the same as the range of the  $W_{R,N,t}^{i,j,l}$  for  $\forall t \in [1, N]$ . We defined  $\tau_{N,t}^{i,j,l}$  mathematically using recursion as follows,

$$\tau_{N,t}^{i,j,l} = \begin{cases} 2^{\binom{l}{2}} \times I^{i,j} & \text{If } 1 \leq t \leq \frac{N}{2^l} \\ 2^{\binom{l}{2}} \times I^{i,j} - 2^{\binom{l}{2}-1} \times (g-1) & \text{If } \frac{N}{2^l} < t \leq \frac{N}{2^{l-1}} \\ \tau_{N,t}^{i,j,l-1} & \text{Else} \end{cases} \quad (15)$$

where  $g$  is the number of gray levels in the image  $M$ .

After performing centre pixel transformation the range of  $\tau_{N,t}^{i,j,l}$  is now matched with the range of  $W_{R,N,t}^{i,j,l}$  for all integer values of  $t$  between 1 and  $N$ . The centre pixel transformed images (i.e.  $\tau_{4,t}^2$ ) for the image of Fig. 5(a) are shown in the Fig. 5(d). The 4 images in this figure are computed for  $t = 1, 2, 3$ , and 4 respectively at level 2 (i.e.  $l = 2$ ), while the number of local neighbors are 4 (i.e.  $N = 4$ ). Visually it is hard to notice the differences between these images but actually the intensity ranges for them are having lot of differences.

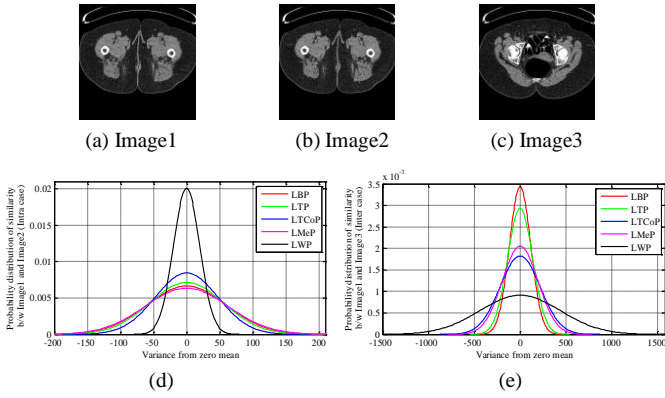


Fig. 6. Examples illustrating the behavior of LBP [21], LTP [27], LTCoP [15], LMeP [17] and LWP for intra and inter class images; (a, b, c) Image1, Image2 and Image3 respectively are three images where Image1 and Image2 are from the same class whereas Image1 and Image3 are from the different classes, (d-e) The probability distributions of the difference of the feature vectors of each method w.r.t. the zero mean for intra (Image1 and Image2) and inter (Image1 and Image3) class images respectively.

#### D. Local Wavelet Pattern

Previously we calculated  $W_{R,N}^{i,j,l}$  by incorporating the relationship among neighboring pixels and  $\tau_N^{i,j,l}$  by range matching of centre pixel with the range of  $W_{R,N}^{i,j,l}$ . Here, in this section, we will use  $W_{R,N}^{i,j,l}$  and  $\tau_N^{i,j,l}$  values to encode the relationship between  $P^{i,j}$  and  $P_{R,N}^{i,j}$  (i.e. between the centre pixel and its neighbors) into binary form. We termed this relation as local wavelet pattern (LWP) which is basically a binary array of  $N$  values corresponding to the each neighbor of  $P^{i,j}$  and defined as follows,

$$LWP_{R,N}^{i,j,l} = [LWP_{R,N,1}^{i,j,l}, LWP_{R,N,2}^{i,j,l}, \dots, LWP_{R,N,N}^{i,j,l}] \quad (16)$$

where  $LWP_{R,N,t}^{i,j,l}$  is a binary LWP value for  $t^{\text{th}}$  neighbor of  $P^{i,j}$  and computed as follows,

$$LWP_{R,N,t}^{i,j,l} = \text{sign}(\Delta_{R,N,t}^{i,j,l}) \quad (17)$$

where  $\text{sign}$  is a function to find that if a number is positive and defined as follows,

$$\text{sign}(\lambda) = \begin{cases} 1, & \text{if } \lambda > 0 \\ 0, & \text{Else} \end{cases} \quad (18)$$

and  $\Delta_{R,N,t}^{i,j,l}$  is the  $t^{\text{th}}$  element of the local wavelet difference at  $l^{\text{th}}$  level for pixel  $P^{i,j}$  and defined as follows,

$$\Delta_{R,N,t}^{i,j,l} = W_{R,N,t}^{i,j,l} - \tau_{N,t}^{i,j,l} \quad (19)$$

We define the local wavelet pattern map (i.e.  $LWPM$ ) for  $P^{i,j}$  using its local wavelet patterns defined in (16) as follows,

$$LWPM_{R,N}^{i,j,l} = \sum_{t=1}^N 2^{t-1} \times LWP_{R,N,t}^{i,j,l} \quad (20)$$

Note that the values of  $LWPM$  is dependent upon the number of neighbors ( $N$ ) considered to form the pattern and it is in between the 0 and  $2^N - 1$ . In other words the range of  $LWPM$  is  $[0, 2^N - 1]$ . We computed the local wavelet

patterns (i.e.  $LWP_{4,4,t}^2 | t = 1, 2, 3, 4$ ) in Fig. 5(e) for an example image considered in the Fig. 5(a) using its local wavelet decomposed images and local pixel transformed images depicted in the Fig. 5(c-d) respectively. The 4 images in the Fig. 5(e) are computed for  $t = 1, 2, 3$ , and 4 when we considered  $l = 2$ ,  $R = 4$  and  $N = 4$ . We also generated the local wavelet pattern map (i.e.  $LWPM_{4,4}^2$ ) for the same example in Fig. 5(b). It is observed that the  $LWPM_{4,4}^2$  map is having more details as compared to the input images which will provide more accurate matching between two images.

#### E. LWP Feature Vector

We computed the local wavelet pattern map ( $LWPM$ ) in previous subsection using proposed local wavelet patterns. The local wavelet pattern feature vector ( $\mathcal{H}$ ) of  $2^N$  dimension is calculated using the  $LWPM$  of every pixels of image  $M$ . We find the LWP feature vector  $\mathcal{H}_{R,N}^l$  at  $l^{\text{th}}$  level of local wavelet decomposition when  $N$  neighbors at radius  $R$  are considered to construct the  $LWPM$  using the following equation,

$$\mathcal{H}_{R,N}^l(\zeta) = \frac{1}{(\widehat{m}_1)(\widehat{m}_2)} \sum_{i=R+1}^{m_1-R} \sum_{j=R+1}^{m_2-R} f_2(LWPM_{R,N}^{i,j,l}, \zeta) \quad (21)$$

for  $\forall \zeta \in [0, 2^N - 1]$ , where,  $m_1 \times m_2$  are the dimension of the image  $M$  (i.e. total number of pixel),  $\widehat{m}_1 = m_1 - 2R$ ,  $\widehat{m}_2 = m_2 - 2R$ , and  $f_2(\alpha, \beta)$  is a function given as follows,

$$f_2(\alpha, \beta) = \begin{cases} 1, & \text{if } \alpha = \beta \\ 0, & \text{Else} \end{cases} \quad (22)$$

We computed and compared the LBP [21], LTP [27], LTCoP [15], LMeP [16] and LWP feature vectors using images of intra and inter categories in Fig. 6. Three images namely Image1, Image2 and Image3 are shown in Fig. 6(a-c) respectively where Image1 and Image2 are taken from the same category and Image1 and Image3 are taken from the different categories of the TCIA-CT database. Fig. 6(d-e) illustrate the probability distributions of the difference of the feature vectors w.r.t. the zero mean for intra (Image1 and Image2) and inter (Image2 and Image3) class images respectively. The y-axis shows the probability that the feature vector of one image differs from another by a particular amount of deviation and x-axis shows the deviation from the zero mean. The large amplitude of probability at zero mean signifies the high similarity between the feature vectors whereas more deviation from zero mean represent the less similar features. In this example, LWP is more discriminative as it better differentiates between Image1 and Image3 while at the same time better matches the Image1 and Image2.

### III. SIMILARITY MEASUREMENT AND EVALUATION CRITERIA

In this section, we present the adopted approach for the similarity measurement and evaluation purpose. The basic aim of similarity measurement is to calculate the distance between the feature vectors of query image and database images. Let the feature vector for two images  $M_a$  and  $M_b$  is denoted as  $\mathcal{H}^a = \{\mathcal{H}^a(1), \mathcal{H}^a(2), \dots, \mathcal{H}^a(dim)\}$  and  $\mathcal{H}^b = \{\mathcal{H}^b(1), \mathcal{H}^b(2), \dots, \mathcal{H}^b(dim)\}$  respectively, where  $dim$  is the length of feature vector and equal to the  $2^N$ . We have



used  $D_1$  similarity measurement technique to find the distance between feature vectors of two images [15] [17]. The  $D_1$  distance measure is defined as,

$$D_1(\mathcal{H}^a, \mathcal{H}^b) = \sum_{\lambda=1}^{dim} \left| \frac{\mathcal{H}^b(\lambda) - \mathcal{H}^a(\lambda)}{1 + \mathcal{H}^b(\lambda) + \mathcal{H}^a(\lambda)} \right| \quad (23)$$

Each database image of  $db$  is considered as a query image and matched with all images. We retrieved the top  $\omega$  matching images using  $d_1$  similarity measure. The approach matches those retrieved images correctly which are retrieved from the same category as of the query image. In order to analyze the performance of the proposed method, we have calculated the average retrieval precision (ARP) and average retrieval rate (ARR) by finding the mean of average precision (AP) and average recall (AR) per category respectively. AP and AR for a particular category is computed by finding the average of precisions and recalls respectively by turning each image of that category as the query image. Let  $\wp(M_j)$  and  $\mathcal{R}(M_j)$  is the precision and recall respectively for the  $j^{th}$  query image (i.e.  $M_j$ ) from category  $\mathcal{C}$  and defined as,

$$\wp(M_j) = \frac{\text{Number of relevant images retrieved}}{\text{Number of images retrieved}} \quad (24)$$

$$\mathcal{R}(M_j) = \frac{\text{Number of relevant images retrieved}}{\text{Number of relevant images in the db}} \quad (25)$$

#### IV. EXPERIMENTS AND COMPARISONS

We devoted this section for medical CT image retrieval experiments and comparisons. We used the ARP and ARR matrices to show the results. Three medical CT image retrieval experiments are performed over publically available TCIA-CT [40], EXACT09-CT [41] and NEMA-CT [42] databases. Until or otherwise specified, we have considered 8 local neighbors ( $N$ ) equally spaced at a radius ( $R$ ) of 1 and applied local wavelet decomposition at  $2^{nd}$  level to construct the LWP

feature vector. We compare the results of LWP feature vector with the results of LBP [21], LTP [27], LDP [45], LMeP [16], LTCoP [15], LTrP [47] and SS-3D-LTP [48] feature vectors. We compared the results over each database in the rest of this section in terms of the efficiency and time complexity. We also compared each method by applying 1)  $u_2$  transformation [49] (i.e. LBPu2, LTPu2, LDPu2, LMePu2, LTCoPu2, LTrPu2, SS-3D-LTPu2 and LWPu2 descriptors), 2) Gabor filter used by Murala et al. [46] (i.e. GLBP, GLTP, GLDP, GLMeP, GLTCoP, GLTrP, GSS-3D-LTP and GLWP descriptors) and 3) both Gabor filter and  $u_2$  transformation (i.e. GLBPu2, GLTPu2, GLDPu2, GLMePu2, GLTCoPu2, GLTrPu2, GSS-3D-LTPu2 and GLWPu2 descriptors).

##### A. Experiment #1

The cancer image archive (TCIA) provides the storage for the huge amount of research, clinical and medical cancer images [40]. These images are made public to download for the purpose of research. Digital Imaging and Communications in Medicine (DICOM) image format is used to store these images. We prepared TCIA-CT database by collecting 604 Colo\_prone 1.0B30f CT images of the DICOM series number 1.3.6.1.4.1.9328.50.4.2 of study instance UID 1.3.6.1.4.1.9328.50.4.1 for subject 1.3.6.1.4.1.9328.50.4.0001. According to the size and structure of Colo\_prone, we manually grouped this collected 604 images into 8 categories having 75, 50, 58, 140, 70, 92, 78, and 41 images respectively. All images are having the dimension of  $512 \times 512$  pixels in this database. Fig. 7 displayed some example images of the TCIA-CT database with one image from each category.

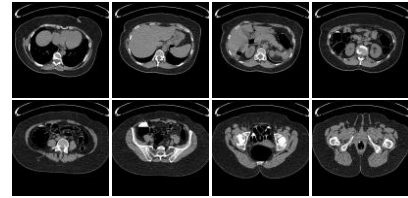


Fig. 7. Some images of TCIA-CT database, one image from each category.

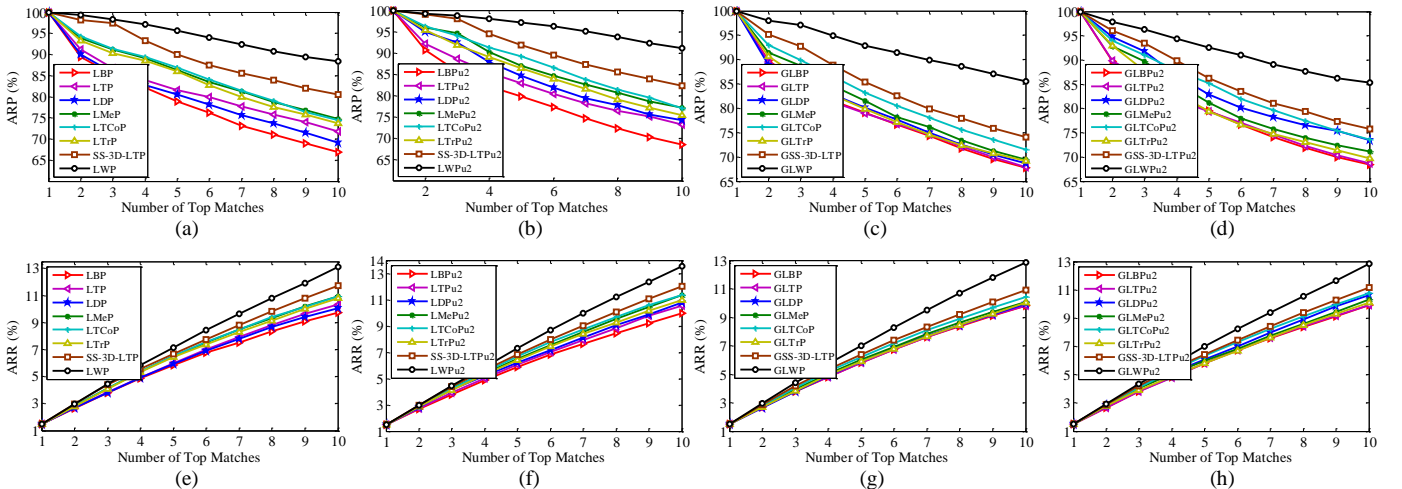


Fig. 8. Illustration of the results in terms of the (a-d) ARP and (e-h) ARR as a function of number of top matches ( $\omega$ ) over TCIA-CT database using (a, e) LBP, LTP, LDP, LMeP, LTCoP, LTrP, SS-3D-LTP and LWP descriptors, (b, f) LBPu2, LTPu2, LDPu2, LMePu2, LTCoPu2, LTrPu2, SS-3D-LTPu2 and LWPu2 descriptors, (c, g) GLBP, GLTP, GLDP, GLMeP, GLTCoP, GLTrP, GSS-3D-LTP and GLWP descriptors, and (d, h) GLBPu2, GLTPu2, GLDPu2, GLMePu2, GLTCoPu2, GLTrPu2, GSS-3D-LTPu2 and GLWPu2 descriptors.

Fig. 8 illustrates the retrieval results in terms of the (a-d) ARP (%) and (e-f) ARR (%) over TCIA-CT database using (a, e) LBP, LTP, LDP, LMeP, LTCoP, LTrP, SS-3D-LTP and LWP descriptors, (b, f) LBPu2, LTPu2, LDPu2, LMePu2, LTCoPu2, LTrPu2, SS-3D-LTPu2 and LWPu2 descriptors, (c, g) GLBP, GLTP, GLDP, GLMeP, GLTCoP, GLTrP, GSS-3D-LTP and GLWP descriptors, and (d, h) GLBPu2, GLTPu2, GLDPu2, GLMePu2, GLTCoPu2, GLTrPu2, GSS-3D-LTPu2 and GLWPu2 descriptors by varying the number of top matches ( $\omega$ ). It is observed from the ARP and ARR results that the performance of the proposed LWP descriptor is better as compared to the performance of the other descriptors.

We also listed the ARP and ARR values in % over this database using each descriptor when  $\omega = 10$  in Table 1. The performance of the LWP is improved by {32.15%, 34.39%}, {23.10%, 26.72%}, {28.03%, 30.25%}, {18.38%, 19.54%}, {18.84%, 19.87%}, {19.96%, 21.54%} and {09.78%, 11.78%} as compared to the LBP, LTP, LDP, LMeP, LTCoP, LTrP and SS-3D-LTP in terms of the {ARP, ARR}. Most of the time, it is desirable for a physician to know the disease category for which any particular method is performing superb or worst. From this point of view, we also reported the results over each category of the database when  $\omega = 10$  using each descriptor in terms of the average precision (AP) in Fig. 9(a) and average recall (AR) in Fig. 9(b). For category 3 the proposed descriptor has gained highest improvement as compared to the other descriptors. The retrieved CT images for a query CT image (see Fig. 10(a)) of TCIA-CT database are shown in the Fig. 10(b) using proposed descriptor. We retrieved top 10 matching images and found that all images are from the same category of the query (i.e. 100% precision is achieved for this example using LWP feature). We have drawn following outcomes on the basis of the results over TCIA-CT database in this experiment:

1. Proposed LWP outperforms LBP, LTP, LMeP, LTCoP, LTrP and SS-3D-LTP in terms of the both ARP (%) and ARR (%).
2. Proposed descriptor also outperforms other descriptors when tested with the Gabor filters,  $u_2$  transformation and both using ARP (%) and ARR (%).
3. The performance of the LWP is also superior in most categories using average precision and average recall.

Table 1. Performance comparison of the descriptors using ARP and ARR values over TCIA-CT database for  $\omega = 10$

Performance	Method							
	LBP	LTP	LDP	LMeP	LTCoP	LTrP	SS-3D-LTP	LWP
ARP (%)	66.91	71.83	69.06	74.69	74.40	73.71	80.54	88.42
ARR (%)	09.74	10.33	10.05	10.95	10.92	10.77	11.71	13.09

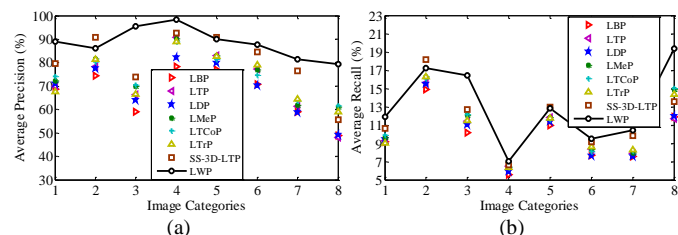


Fig. 9. Categorical performance comparison of each descriptor in terms of the (a) average precision and (b) average recall over TCIA-CT database when  $\omega = 10$ .

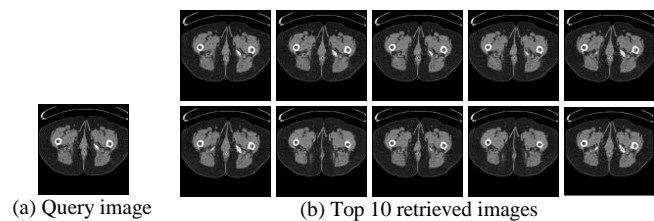


Fig. 10. The retrieved images using LWP for a query from TCIA-CT database.

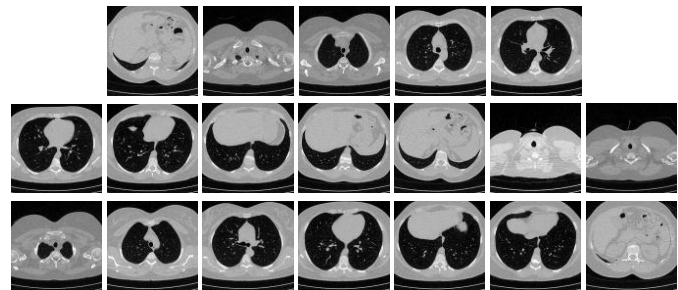


Fig. 11. EXACT09-CT example images, one image from each group.

## B. Experiment #2

Extraction of Airways from CT 2009 (EXACT09) is a database of chest CT scans [41]. This database contains the images in two sets training and testing with 20 cases in each set. The DICOM format is used to store the CT scan images. We considered the 675 CT images of CASE23 of testing set of EXACT09 in this paper for image retrieval experiment and grouped these images on the basis of the structure and size of CT scans into 19 categories having 36, 23, 30, 30, 50, 42, 20, 45, 50, 24, 28, 24, 35, 40, 50, 35, 30, 28 and 55 CT images to form the EXACT09-CT database. The dimension of the images is  $512 \times 512$ . Fig. 11 depicts the example images of EXACT09-CT database with one image of each group.

The performance comparison among LBP, LTP, LDP, LMeP, LTCoP, LTrP, SS-3D-LTP and LWP feature descriptors (including the descriptors with Gabor filter,  $u_2$  transformation and both) are made in Fig. 12(a-h) over EXACT09-CT database in terms of the ARP and ARR as a function of  $\omega$ . The performance gain of LWP over LTCoP decreases under  $u_2$  transformation while it increases when Gabor filters are used. Table 2 summarized the ARP and ARR values using LBP, LTP, LDP, LMeP, LTCoP, LTrP, SS-3D-LTP and LWP feature descriptors when  $\omega = 10$ . It is evident from Fig. 12 and Table 2 that the performance of LWP is better as compared to the other descriptors. Fig. 13 depicts the top 10 retrieved images with 100% precision for a query image from the EXACT09-CT database. The following inferences are gathered over the EXACT09-CT database:

1. The ARP using proposed LWP is improved by 27.63%, 33.68%, 52.57%, 31.27%, 12.96%, 43.55% and 23.88% of the ARPs using LBP, LTP, LDP, LMeP, LTCoP, LTrP and SS-3D-LTP respectively when  $\omega = 10$ .
2. The ARR using proposed LWP is improved by 27.47%, 34.14%, 53.61%, 31.52%, 12.23%, 43.84% and 23.79% of the ARRs using LBP, LTP, LDP, LMeP, LTCoP, LTrP and SS-3D-LTP respectively when  $\omega = 10$ .
3. LWP outperforms the state-of-the-art descriptors under a) Gabor filter, b)  $u_2$  transformation and 3) both Gabor filter and  $u_2$  transformation.

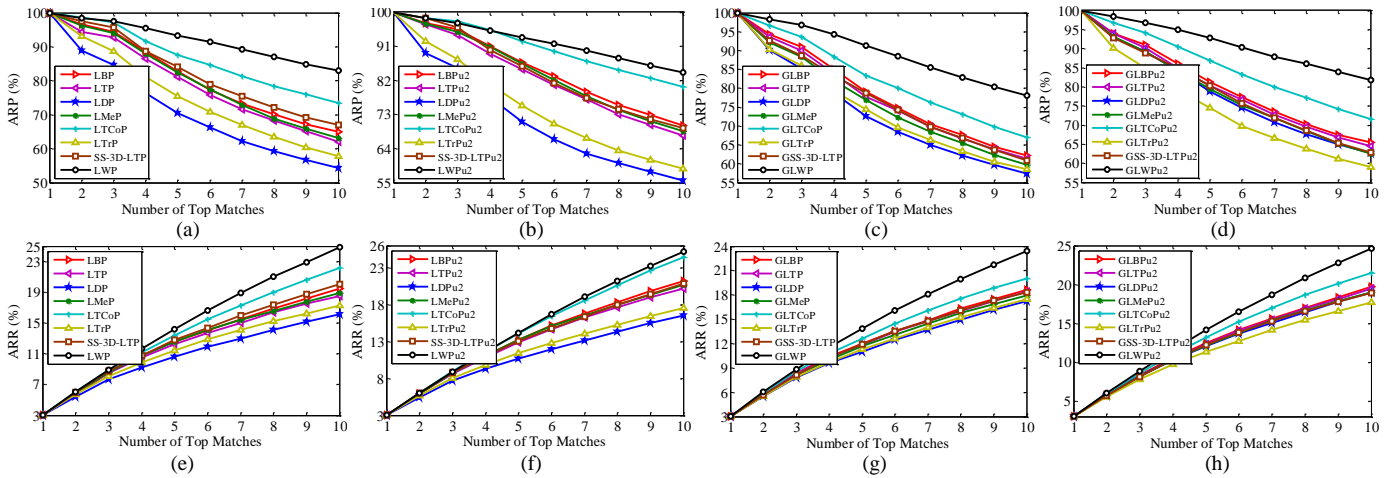


Fig. 12. Performance comparison of our descriptor with other descriptors by considering the (a-d) ARP and (e-h) ARR evaluation criteria and number of top matches over EXACT09-CT database using (a, e) LBP, LTP, LDP, LMeP, LTCoP, LTrP, SS-3D-LTP and LWP descriptors, (b, f) LBPu2, LTPu2, LDPu2, LMePu2, LTCoPu2, LTrPu2, SS-3D-LTPu2 and LWPu2 descriptors, (c, g) GLBP, GLTP, GLDP, GLMeP, GLTCoP, GLTrP, GSS-3D-LTP and GLWP descriptors, and (d, h) GLBPu2, GLTPu2, GLDPu2, GLMePu2, GLTCoPu2, GLTrPu2, GSS-3D-LTPu2 and GLWPU2 descriptors.

Table 2. Results comparison among different descriptors using ARP and ARR values over EXACT09-CT database for  $\omega = 10$

Performance	Method							
	LBP	LTP	LDP	LMeP	LTCoP	LTrP	SS-3D-LTP	LWP
ARP (%)	65.03	62.09	54.40	63.23	73.48	57.82	67.00	83.00
ARR (%)	19.51	18.54	16.19	18.91	22.16	17.29	20.09	24.87

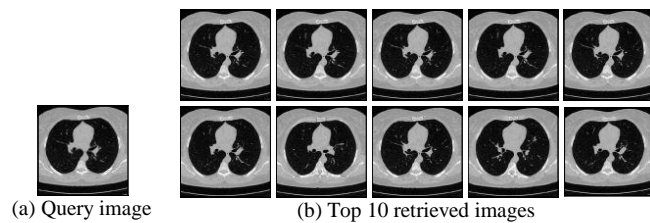


Fig. 13. Retrieved images using proposed descriptor for a query image of EXACT09-CT database.

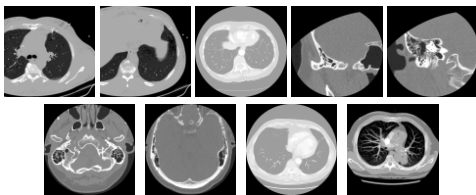


Fig. 14. Example images of NEMA-CT database, one image from each category is shown.

### C. Experiment #3

The digital imaging and communications in medicine (DICOM) standard are created by the National Electrical Manufacturers Association (NEMA) [42] in order to assist the storage and uses of medical images for research and diagnosis purpose. We considered the CT0001, CT0003, CT0057, CT0060, CT0080, CT0082, and CT0083 cases of this database in this paper. We collected 315 CT images (dimension: 512x512) of different parts of the body from NEMA database in this experiment and categorized it into 9 categories having 36, 18, 36, 37, 41, 30, 23, 70 and 24 images to form the NEMA-CT database. Fig. 14 shows one sample image from each category of this database.

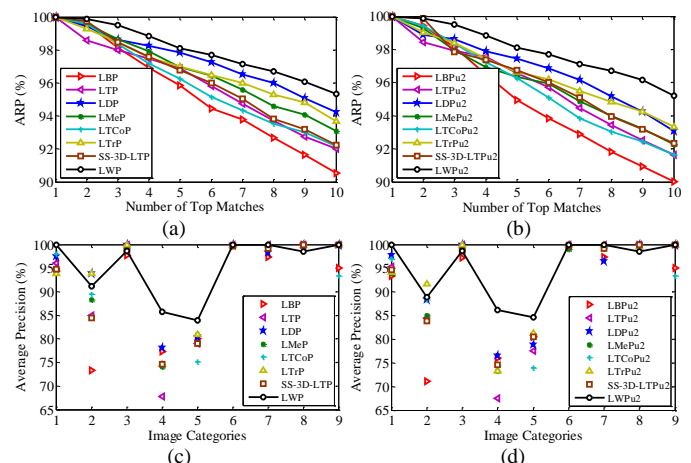


Fig. 15. Results comparison of LWP with LBP, LTP, LMeP, LTCoP, LTrP and SS-3D-LTP over NEMA-CT database in terms of the (a) ARP vs  $\omega$ , (b) ARP vs  $\omega$  under  $u_2$  transformation, (c) average precision vs category, and (d) average precision vs category under  $u_2$  transformation.

Table 3. Results comparison of different methods in terms of ARP and ARR over NEMA-CT database when  $\omega = 10$

Performance	Method							
	LBP	LTP	LDP	LMeP	LTCoP	LTrP	SS-3D-LTP	LWP
ARP (%)	90.55	92.00	94.22	93.09	92.15	93.69	92.24	95.32
ARR (%)	29.33	30.23	31.08	30.62	30.31	30.96	30.26	31.33

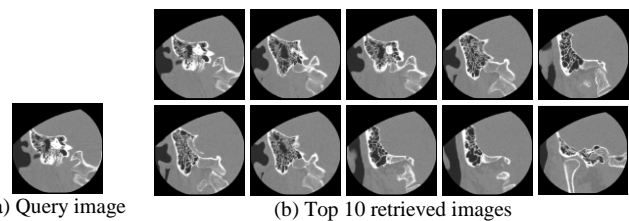


Fig. 16. Retrieved images using LWP feature vector for a query image of NEMA-CT database. 100% precision is gained in this example.

We have illustrated the results comparison among each descriptor over NEMA-CT database in terms of the ARP by varying the number of top matches in the Fig. 15(a). The



performance comparison among these descriptors are also presented for each category of the NEMA-CT database in Fig. 15(c) in terms of the average precision when the number of top matches are 10 (i.e.  $\omega = 10$ ). The ARP and average precision are also compared under  $u_2$  transformation of each descriptor in Fig. 15(b) and Fig. 15(d) respectively. It is discovered from the Fig. 15 that LWP feature vector is well suited for the medical CT image retrieval when images are taken from the different part of the body also. We listed the values of ARP as well ARR in the Table 3 for each feature descriptor over NEMA-CT database when  $\omega = 10$ . It can be observed that the performance of the LWP is improved as compared to the performance of the LBP, LTP, LDP, LMeP, LTCoP, LTrP and SS-3D-LTP. Fig. 16(b) shows 10 retrieved images for a query image of Fig. 16(a) with 100% precision. From the experimental results over NEMA-CT database, we have ended with the following assertions:

1. The retrieval performance of the proposed LWP feature descriptor is improved significantly as compared to the performance of the LBP, LTP, LDP, LMeP, LTCoP, LTrP and SS-3D-LTP feature descriptors over NEMA-CT database.
2. The proposed descriptor also outperforms other descriptor under  $u_2$  transformation in terms of the ARP and average precision over NEMA-CT database.
3. NEMA-CT database is composed of the categories from the different part of body and LWP performs better in most of categories of this database.

#### D. Performance V/S Time Complexity

We depicted the total feature extraction time and total retrieval time in seconds in Fig. 17 using LBP ( $dim: 256$ ), LTP ( $dim: 2 \times 256$ ), LDP ( $dim: 4 \times 256$ ), LMeP ( $dim: 3 \times 256$ ), LTCoP ( $dim: 2 \times 256$ ), LTrP ( $dim: 13 \times 256$ ), SS-3D-LTP ( $dim: 10 \times 256$ ), and LWP ( $dim: 256$ ) feature descriptors over each database. The total feature extraction time is computed by calculating the total time required to extract a particular feature over all the images of that database. The total retrieval time over a particular database is computed by finding the total time required to match each image of that dataset with remaining images. All the experiments are conducted using a system having Intel(R) Core(TM) i5 CPU 650@3.20 GHz processor, 4 GB RAM, and 32-bit Windows 7 Ultimate operating system. We observed that the feature extraction time of LWP is better than LDP, LTCoP, LTrP and SS-3D-LTP descriptors. We also found that the retrieval time of LWP is nearly equal as compared to the LBP.

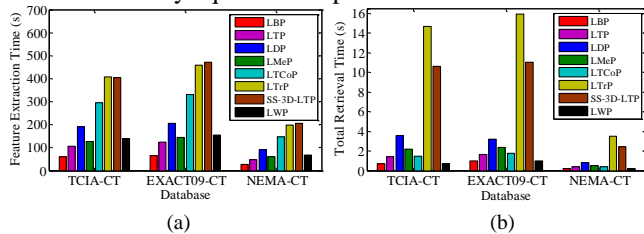


Fig. 17. (a) Total Feature Extraction Time and (b) Total retrieval time in seconds over TCIA-CT, EXACT09-CT and NEMA-CT databases using LBP ( $dim: 256$ ), LTP ( $dim: 2 \times 256$ ), LDP ( $dim: 4 \times 256$ ), LMeP ( $dim: 3 \times 256$ ), LTCoP ( $dim: 2 \times 256$ ), LTrP ( $dim: 13 \times 256$ ), SS-3D-LTP ( $dim: 10 \times 256$ ), and LWP ( $dim: 256$ ) feature vectors.

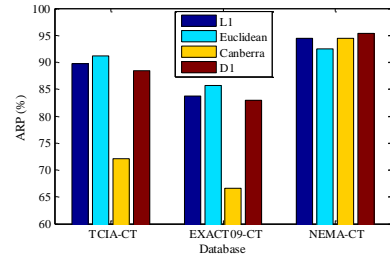


Fig. 18. The results comparison for different similarity measures in terms of the ARP (for  $\omega = 10$ ) using LWP feature vector.

The total retrieval time using LWP is lowered by nearly 2.25, 1.67 and 1.88 times over TCIA-CT, EXACT09-CT, and NEMA-CT databases respectively as compared to the LTP and LTCoP. A significant improvement of nearly 3 times less in total retrieval time using LWP is also observed as compared to the LMeP. The LWP outperforms the LDP, LTCoP, LTrP and SS-3D-LTP in terms of the both feature extraction as well as retrieval time. We have already seen that the performance of LWP is also better than the LBP, LTP, LDP, LMeP, LTCoP, LTrP and SS-3D-LTP. We can say that LWP is more efficient in terms of both performance and time complexity as compared to the existing approaches.

## V. RESULT ANALYSIS AND DISCUSSIONS

In this section, we performed the result analysis using LWP feature vector from different aspects and discussed in details. First, we have shown the behavior of LWP with different similarity measures, then we illustrated the impact of the level of wavelet decomposition over the performance of the LWP feature descriptor, and finally we analyzed the results for different radius of local neighborhood used in the construction of the LWP feature vector. In the last of this section, we also analyzed the effect of local neighborhood population over the performance of LWP descriptor.

### A. Effect of Similarity Measures

As far in this paper, we used the  $D_1$  similarity measure to find the similarity between the descriptors of two images. Here, we show the effect of similarity measures over the performance of the LWP feature descriptor. The comparison among the performances using Euclidean,  $L_1$ , Canberra and  $D_1$  similarity measures are shown in the Fig. 18 over TCIA-CT, EXACT09-CT, and NEMA-CT databases with LWP feature vector in terms of the ARP vs  $\omega$ . The Euclidean,  $L_1$  and Canberra similarity measures are defined in [15]. We found that Canberra similarity measure is worst with LWP feature descriptor. The performance with Euclidean similarity measures is best over TCIA-CT and EXACT09-CT databases but it drastically fails over NEMA-CT database. The performances of LWP feature vector using  $L_1$  and  $D_1$  similarity measures are better over each dataset. We used  $D_1$  similarity measure previously because the other methods have also used this similarity measure. The  $D_1$  similarity measure will be used in rest of the analysis of this paper. It is also observed that the performance of LWP with different similarity measures is similar over TCIA-CT and EXACT09-CT databases (i.e. databases from the same portion of the body) while it is different over NEMA-CT database (i.e.

database from the different portion of the body). It is preferable to use the Euclidean distance for TCIA-CT and EXACT09-CT and  $D_1$  distance for NEMA-CT database.

### B. Effect of Level of Wavelet Decomposition

We also analyzed the effect of level ( $l$ ) of local wavelet decomposition over the performance of the LWP descriptor. For 8 local neighbors at 1 radius of neighborhood (i.e.,  $N = 8$  and  $R = 1$ ), the maximum possible value of  $l$  is 3 (i.e.,  $l_{max} = 3$ ) according to (6). We tested the LWP descriptor for  $l = 1, 2$ , and 3 in the Fig. 19(a-c) over TCIA-CT, EXACT09-CT and NEMA-CT databases respectively. It is observed across the plots of the Fig. 19 that the performance of LWP is nearly increasing over TCIA-CT and EXACT09-CT databases with the increase in  $l$ . In the case of NEMA-CT database, the performance of LWP is better for  $l = 1$ . This was the fact that we used  $l = 2$  for LWP in the results so far and we will also use  $l = 2$  for LWP in the rest of the analysis of this paper. From this analysis, it is desirable to use the higher level of wavelet decomposition for the databases having images from the same body part such as TCIA-CT and EXACT09-CT database and the lower level of wavelet decomposition for the databases having images from the different body part such as NEMA-CT database. Moreover, the dimension of the LWP descriptor doesn't change with the level of wavelet decomposition which is a major finding of our approach.

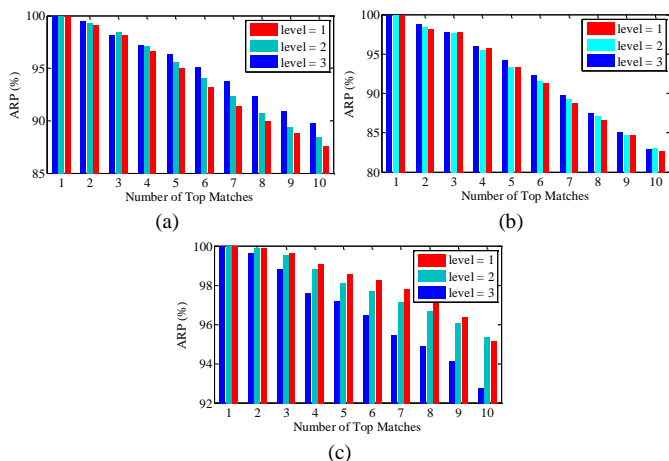


Fig. 19. The results comparison for different levels of wavelet decomposition of LWP descriptor in terms of the ARP vs  $\omega$  over (a) TCIA-CT, (b) EXACT09-CT, and (c) NEMA-CT databases. The values of  $N$  and  $R$  are 8 and 1 in this analysis so the possible levels of wavelet decomposition are 1, 2 and 3.

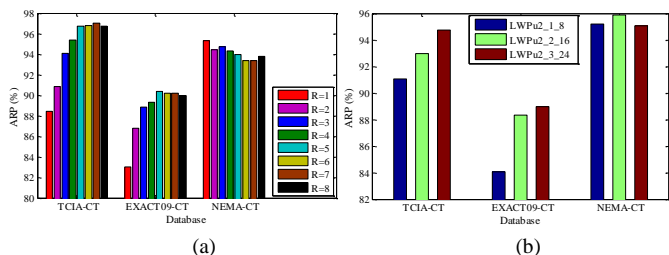


Fig. 20. (a) The impact of the radius of local neighborhood ( $R$ ) over the performance of the LWP descriptor in terms of the ARP (for  $\omega = 10$ ). The values of number of local neighbors ( $N$ ) and level of wavelet decomposition ( $l$ ) are 8 and 2 in this analysis. (b) The effect of population (i.e. number of neighbors,  $N$ ) of local neighborhood over the ARP (for  $\omega = 10$ ) using LWPu2 descriptor.

### C. Effect of Radius of Local Neighborhood

In order to know the effect of radius of local neighborhood ( $R$ ) over the performance of the LWP feature descriptor, we performed an analysis by considering the values of  $R$  from 1 to 8 over TCIA-CT, EXACT09-CT and NEMA-CT databases in the Fig. 20(a) in terms of the ARP for  $\omega = 10$ . It is deduced that the performance of LWP feature descriptor is generally improving with the increase in  $R$  except over NEMA-CT database. It is also observed that the performance of LWP saturates for the larger values of  $R$  (such as 6, 7 and 8) except over NEMA-CT database. We have used  $R = 1$  in the rest of the paper. However, it is discovered that the performance of LWP feature descriptor with  $R = 5$  is far better as compared to the performance of LWP with  $R = 1$  over TCIA-CT and EXACT09-CT databases. From this discussion, it is pointed out that larger radius of local neighborhood will be more useful in the cases where the databases are containing the images having less inter class variations such as TCIA-CT and EXACT09-CT databases while lower radius of local neighborhood is preferable for databases having more inter class variations. The dimension of the LWP descriptor is invariant to the radius of the local neighborhood used to construct the descriptor.

### D. Effect of Local Neighborhood Population

We have demonstrated the ARP values in Fig. 20(b) over each database by varying the number of neighbors (i.e. population of local neighborhood,  $N$ ) with respect to the radius ( $R$ ) of neighborhood. The LWPu2\_R\_N represents the u2 transformation of the LWP descriptor extracted over the local neighborhood at a radius of  $R$  with population size  $N$ . The number of top matches is considered as 10 in the plot of Fig. 20(b). From this result, it is noticed that the performance of proposed descriptor is also depends over the population size and generally increases with more number of local neighbors such as in the case of the TCIA-CT and EXACT09-CT databases.

From the results of the Fig. 18-20, it is evident that the performance of the LWP is similar over the databases having images from the same body part such as the cases of the TCIA-CT and EXACT09-CT databases while it is slight different over the database of different body part such as the case of NEMA-CT database. From the experimental results in terms of ARP, ARR, average precision, average recall and total retrieval time and discussions over TCIA-CT, EXACT09-CT and NEMA-CT databases, it is pointed out that proposed LWP feature descriptor is more discriminative and efficient as compared to the LBP, LTP, LMeP, LTCoP, LTrP and SS-3D-LTP feature descriptors. We also analyzed that the performance of the proposed method is increasing with the increase in the radius of the local neighborhood, whereas its dimension remains constant.

## VI. CONCLUSION

We proposed a new local wavelet pattern (LWP) based image feature descriptor in this paper for medical CT image retrieval. First of all, the local wavelet decomposition is performed over local neighborhood of any pixel to encode the relation among the neighboring pixel. Then, the local wavelet

decomposed values are compared with the transformed values of the centre pixel to encode the relation between the centre and neighboring pixels and computed the LWP pattern for the centre pixel. The introduced LWP is constructed for each pixel of the image and finally used to find the histogram as a feature vector. In order to test the LWP feature descriptor, we performed three medical CT image retrieval experiments and in each experiment we compared the LWP with the LBP, LTP, LMeP, LTCoP, LTrP and SS-3D-LTP feature descriptors. From the experiments, we found that the proposed feature descriptor outperforms the existing feature descriptors over each database. We also observed that the performance of LWP is better for nearly each category of the each database. We also analyzed that the time complexity of the proposed feature descriptor is also less. The dimension of LWP only depends upon the number of local neighbors considered in the construction process. It is also examined that the performance of the LWP descriptor is improving with the increase in the radius of the local neighborhood. It is evident from the experiments and analysis that the proposed LWP feature descriptor is more efficient as well as more discriminative and can be used effectively for the medical CT image diagnosis.

## REFERENCES

- [1] D. L. Rubin, H. Greenspan, and J. F. Brinkley, "Biomedical Imaging Informatics," *Biomedical Informatics*, pp. 285-327, 2014. Springer London.
- [2] M. Flickner, H. Sawhney, W. Niblack, J. Ashley, Q. Huang, B. Dom, M. Gorkani, J. Hafner, D. Lee, D. Petkovic, D. Steele, and P. Yanker, "Query by image and video content: The QBIC system," *Computer*, vol. 28, no. 9, pp. 23-32, 1995.
- [3] A.W.M. Smeulders, M. Worring, S. Santini, A. Gupta, and R. Jain, "Content-based image retrieval at the end of the early years," *IEEE Trans. Pattern Anal. Mach. Intell.*, vol. 22, no. 12, pp. 1349-1380, Dec. 2000.
- [4] Y. Liu, D. Zhang, G. Lu, and W. Y. Ma, "A survey of content-based image retrieval with high-level semantics," *Pattern Recog.*, vol. 40, pp. 262-282, 2007.
- [5] H. Muller, A. Rosset, J. P. Vallee, and A. Geisbuhler, "Comparing feature sets for content-based image retrieval in a medical case database," in *Proc. SPIE Med. Imag., PACS Imag. Inf.*, 2004, pp. 99 - 109.
- [6] L. Zheng, A.W. Wetzel, J. Gilbertson, and M.J. Becich, "Design and analysis of a content-based pathology image retrieval system," *IEEE Trans. Inf. Tech. Biomed.*, vol. 7, no. 4, pp. 249-255, 2003.
- [7] A. Quddus and O. Basir, "Semantic image retrieval in magnetic resonance brain volumes," *IEEE Trans. Inf. Tech. Biomed.*, vol. 16, no. 3, pp. 348-355, 2012.
- [8] X. Xu, D. J. Lee, S. Antani, and L. R. Long, "A Spine X-Ray image retrieval system using partial shape matching," *IEEE Trans. Inf. Tech. Biomed.*, vol. 12, no. 1, pp. 100-108, 2008.
- [9] H. C. Akakin and M. N. Gurcan, "Content-Based microscopic image retrieval system for multi-image queries," *IEEE Trans. Inf. Tech. Biomed.*, vol. 16, no. 4, pp. 758-769, 2012.
- [10] M. M. Rahman, S. K. Antani and G. R. Thoma, "A learning-based similarity fusion and filtering approach for biomedical image retrieval using SVM classification and relevance feedback," *IEEE Trans. Inf. Tech. Biomed.*, vol. 15, no. 4, pp. 640-646, 2011.
- [11] G. Scott and C. R. Shyu, "Knowledge-Driven multidimensional indexing structure for biomedical media database retrieval," *IEEE Trans. Inf. Tech. Biomed.*, vol. 11, no. 3, pp. 320-331, 2007.
- [12] H. Muller, N. Michoux, D. Bandon, and A. Geisbuhler, "A review of content-based image retrieval systems in medical applications - Clinical benefits and future directions," *J. Med. Inf.*, vol. 73, no. 1, pp. 1-23, 2004.
- [13] A. B. L. Larsen, J. S. Vestergaard, and R. Larsen, "HEp-2 cell classification using shape index histograms with donut-shaped spatial pooling," *IEEE Trans. Med. Imag.*, vol. 33, no. 7, pp. 1573-1580, 2014.
- [14] F. S. Zakeri, H. Behnam, and N. Ahmadinejad, "Classification of benign and malignant breast masses based on shape and texture features in sonography images," *J. Med. Syst.*, vol. 36, no. 3, pp. 1621-1627, 2012.
- [15] S. Murala and Q. M. J. Wu, "Local ternary and co-occurrence patterns: A new feature descriptor for MRI and CT image retrieval," *Neurocomputing*, vol. 119, pp. 399-412, 2013.
- [16] S. Murala and Q. M. J. Wu, "Local Mesh Patterns Versus Local Binary Patterns: Biomedical Image Indexing and Retrieval," *IEEE Journal of Biomedical and Health Informatics*, vol.18, no.3, pp. 929-938, 2014.
- [17] M. M. Rahman, P. Bhattacharya, and B. C. Desai, "A framework for medical image retrieval using machine learning and statistical similarity matching techniques with relevance feedback," *IEEE Transactions on Information Technology in Biomedicine*, vol. 11, no. 1, pp. 58-69, 2007.
- [18] R. Rahmani, S. A. Goldman, H. Zhang, S. R. Cholleti, and J. E. Fritts, "Localized content-based image retrieval," *IEEE Transactions on Pattern Analysis and Machine Intelligence*, vol. 30, no. 11, pp. 1902-1912, 2008.
- [19] V. Khanh, K. A. Hua, and W. Tavanapong, "Image retrieval based on regions of interest," *IEEE Transactions on Knowledge and Data Engineering*, vol. 15, no. 4, pp. 1045-1049, 2003.
- [20] K. Konstantinidis, A. Gasteratos, I. Andreadis, "Image retrieval based on fuzzy color histogram processing," *Optics Communications*, vol. 248, no. 4-6, pp. 375-386, 2005.
- [21] T. Ojala, M. Pietikainen, and D. Harwood, "A comparative study of texture measures with classification based on feature distributions," *Pattern Recog.*, vol. 29, no. 1, pp. 51-59, 1996.
- [22] T. Ahonen, A. Hadid, and M. Pietikainen, "Face description with local binary patterns: Applications to face recognition," *IEEE Trans. Pattern Anal. Mach. Intell.*, vol. 28, no. 12, pp. 2037-2041, 2006.
- [23] S. He, J. J. Soraghan, B. F. O'Reilly, and D. Xing, "Quantitative analysis of facial paralysis using local binary patterns in biomedical videos," *IEEE Trans. Biomed. Eng.*, vol. 56, no. 7, pp. 1864-1870, 2009.
- [24] L. Sorensen, S. B. Shaker, and M. de Bruijne, "Quantitative analysis of pulmonary emphysema using local binary patterns," *IEEE Trans. Med. Imag.*, vol. 29, no. 2, pp. 559-569, 2010.
- [25] T. Ojala, M. Pietikainen, and T. Maenpaa, "Multiresolution gray-scale and rotation invariant texture classification with local binary patterns," *IEEE Trans. Pattern Anal. Mach. Intell.*, vol. 24, no. 7, pp. 971-987, 2002.
- [26] M. Heikkil, M. Pietikainen, and C. Schmid, "Description of interest regions with local binary patterns," *Pattern Recog.*, vol. 42, pp. 425-436, 2009.
- [27] X. Tan and B. Triggs, "Enhanced local texture feature sets for face recognition under difficult lighting conditions," *IEEE Trans. Image Process.*, vol. 19, no. 6, pp. 1635-1650, 2010.
- [28] S. R. Dubey, S. K. Singh, and R. K. Singh, "A multi-channel based illumination compensation mechanism for brightness invariant image retrieval," *Multimedia Tools and Applications*, pp. 1-31, 2014.
- [29] S. Peng, D. Kim, S. Lee, and M. Lim, "Texture feature extraction on uniformity estimation for local brightness and structure in chest CT images," *J. Comput. Biol. Med.*, vol. 40, pp. 931-942, 2010.
- [30] D. Unay, A. Ekin, and R.S. Jasinschi, "Local structure-based region-of-interest retrieval in brain MR images," *IEEE Trans. Inf. Tech. Biomed.*, vol. 14, no. 4, pp. 897-903, 2010.
- [31] B. Li and M. Q. H. Meng, "Tumor recognition in wireless capsule endoscopy images using textural features and SVM-Based feature selection," *IEEE Trans. Inf. Tech. Biomed.*, vol. 16, no. 3, pp. 323-329, 2012.
- [32] J. C. Felipe, A. J. M. Traina, and C. Traina Jr., "Retrieval by content of medical images using texture for tissue identification," in *Proc. 16th IEEE Symp. Comput.-Based Med. Syst.*, 2003, pp. 175-180.
- [33] W. Cai, D. D. Feng, and R. Fulton, "Content-based retrieval of dynamic PET functional images," *IEEE Trans. Inf. Tech. Biomed.*, vol. 4, no. 2, pp. 152-158, 2000.
- [34] L. Yang, Student, R. Jin, L. Mummert, R. Sukthankar, A. Goode, B. Zheng, S. C. H. Hoi, and M. Satyanarayanan, "A boosting framework for visibility-preserving distance metric learning and its application to medical image retrieval," *IEEE Trans. Pattern Anal. Mach. Intell.*, vol. 32, no. 1, pp. 33-44, 2010.
- [35] I. El-Naqa, Y. Yang, N. P. Galatsanos, R. M. Nishikawa, and M. N. Wernick, "A similarity learning approach to content-based image retrieval: application to digital mammography," *IEEE Trans. Med. Imag.*, vol. 23, no. 10, pp. 1233-1244, 2004.
- [36] B. Andr e, T. Vercauteren, A. M. Buchner, M. B. Wallace, and N. Ayache, "Learning semantic and visual similarity for endomicroscopy

- video retrieval,” *IEEE Trans. Med. Imag.*, vol. 31, no. 6, pp. 1276–1288, Jun. 2012.
- [37] G. Quellec, M. Lamard, G. Cazuguel, B. Cochener, and C. Roux, “Wavelet optimization for content-based image retrieval in medical databases,” *J. Med. Image Anal.*, vol. 14, pp. 227-241, 2010.
- [38] A. Traina, C. Castanon, and C. Traina Jr., “Multiwavemed: a system for medical image retrieval through wavelets transformations,” in Proc. 16th *IEEE Symp. Comput.-Based Med. Syst.*, 2003, pp. 150 -155.
- [39] E. Stollnitz, T. DeRose, and D. Salesin, “*Wavelet for computer graphics: Theory and applications*,” Los Altos, CA: Morgan Kaufmann, 1996.
- [40] K. Clark, B. Vendt, K. Smith, J. Freymann, J. Kirby, P. Koppel, S. Moore, S. Phillips, D. Maffitt, M. Pringle, L. Tarbox, and F. Prior, “The Cancer Imaging Archive (TCIA): Maintaining and Operating a Public Information Repository,” *Journal of Digital Imaging*, vol. 26, no. 6, pp. 1045-1057, 2013.
- [41] P. Lo, B. Van Ginneken, J. M. Reinhardt, T. Yavarna, P. A. De Jong, B. Irving, ... and M. De Bruijne, “Extraction of airways from CT (EXACT’09),” *IEEE Transactions on Medical Imaging*, vol. 31, no. 11, pp. 2093-2107, 2012.
- [42] NEMA-CT image database, Available from [Online]: <ftp://medical.nema.org/medical/Dicom/Multiframe/>.
- [43] S. R. Dubey, S. K. Singh, and R. K. Singh, “Rotation and Illumination Invariant Interleaved Intensity Order Based Local Descriptor,” *IEEE Transactions on Image Processing*, vol. 23, no. 12, pp. 5323-5333, 2014.
- [44] S. R. Dubey, S. K. Singh, and R. K. Singh, “Local Diagonal Extrema Pattern: A New and Efficient Feature Descriptor for CT Image Retrieval,” *IEEE Signal Processing Letters*, vol. 22, no. 9, pp. 1215-1219, 2015.
- [45] B. Zhang, Y. Gao, S. Zhao, and J. Liu, “Local derivative pattern versus local binary pattern: face recognition with high-order local pattern descriptor,” *IEEE Transactions on Image Processing*, vol. 19, no. 2, pp. 533-544, 2010.
- [46] S. Murala, A. B. Gonde, and R. P. Maheshwari, “Color and texture features for image indexing and retrieval,” *In the proceedings of the IEEE International Advance Computing Conference*, pp. 1411-1416, 2009.
- [47] S. Murala, R. P. Maheshwari, and R. Balasubramanian, “Local tetra patterns: a new feature descriptor for content-based image retrieval,” *IEEE Transactions on Image Processing*, vol. 21, no. 5, pp. 2874-2886, 2012.
- [48] S. Murala and Q. M. Jonathan Wu, “Spherical symmetric 3D local ternary patterns for natural, texture and biomedical image indexing and retrieval,” *Neurocomputing*, vol. 149, pp. 1502-1514, 2015.
- [49] Z. Guo, L. Zhang, and D. Zhang, “Rotation invariant texture classification using LBP variance (LBPV) with global matching,” *Pattern recognition*, vol. 43, no. 3, pp. 706-719, 2010.
- [50] S. R. Dubey, S. K. Singh, and R. K. Singh, “Local Bit-plane Decoded Pattern: A Novel Feature Descriptor for Biomedical Image Retrieval,” *IEEE Journal of Biomedical and Health Informatics*, 2015.